Inorganic Chemistry
Cite This: Inorg. Chem. XXXX, XXX, XXX–XXX
Article
pubs.acs.org/IC

Highly Cytotoxic Ruthenium(II)-Arene Complexes from Bulky 1-Pyrenylphosphane Ligands

Rosa F. Brissos,[†] Pau Clavero,[†] Albert Gallen,[†] Arnald Grabulosa,*[,†] Leoní A. Barrios, Ana B. Caballero,[†] Luís Korrodi-Gregório,[‡] Ricardo Pérez-Tomás,[‡] Guillermo Muller,[†] Vanessa Soto-Cerrato,[‡] and Patrick Gamez*[,†,§,⊥]

[†]Department of Inorganic and Organic Chemistry, Inorganic Chemistry Section, University of Barcelona, Martí i Franquès 1-11, 08028 Barcelona, Spain

[‡]Department of Pathology and Experimental Therapeutics, Faculty of Medicine, University of Barcelona, Campus Bellvitge, Feixa Llarga s/n, 08907 L'Hospitalet de Llobregat, Spain

[§]Catalan Institution for Research and Advanced Studies (ICREA), Passeig Lluís Companys 23, 08010 Barcelona, Spain

[⊥]Institute of Nanoscience and Nanotechnology (IN2UB), Universitat de Barcelona, 08028 Barcelona, Spain

Supporting Information

ABSTRACT: In the present study, the potential anti-neoplastic properties of a series of ruthenium half-sandwich complexes of formula [Ru(η^6-arene)Cl_2(PR^1R^2(1-pyrenyl))] (η^6-arene = *p*-cymene and R^1 = R^2 = methyl for **1**; η^6-arene = methylbenzoate and R^1 = R^2 = methyl for **2**; η^6-arene = *p*-cymene and R^1 = R^2 = phenyl for **3**; η^6-arene = methylbenzoate and R^1 = R^2 = phenyl for **4**; η^6-arene = *p*-cymene, R^1 = methyl and R^2 = phenyl for **5**; η^6-arene = methylbenzoate, R^1 = methyl and R^2 = phenyl for **6**) have been investigated. The six structurally related organoruthenium(II) compounds have been prepared in good yields and fully characterized; the X-ray structures of three of them, i.e., **1**, **2**, and **4**, were determined. Although the piano-stool compounds contain a large polycyclic aromatic moiety, viz. a 1-pyrenyl group, they do not appear to interact with DNA. However, all the piano-stool complexes show significant cytotoxic properties against five human cell lines, namely, lung adenocarcinoma (A549), melanoma (A375), colorectal adenocarcinoma (SW620), breast adenocarcinoma (MCF7), and nontumorigenic epithelial breast (MCF10A), with IC_{50} values in the micromolar range for most of them. In addition, the most active compound, i.e., **2**, induces a remarkable decrease of cell viability, that is in the nanomolar range, against two human neuroblastoma cell lines, namely, SK-N-BE(2) and CHLA-90. Complexes **1**−**6** are all capable of inducing apoptosis, but with various degrees of magnitude. Whereas **1**, **3**, **5**, and **6** have no effect on the cell cycle of A375 cells, **2** and **4** can arrest it at the G_2/M phase; furthermore, **2** (which is the most efficient compound of the series) also stops the cycle at the S phase, behaving as the well-known anticancer agent cisplatin. Finally, **2** is able to inhibit/reduce the cell migration of neuroblastoma SK-N-BE(2) cells.

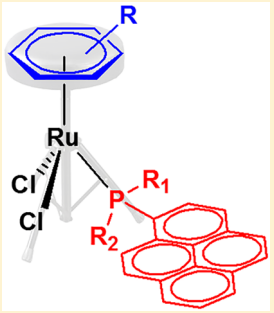

INTRODUCTION

Cancer is a major global health problem, which represents the second leading cause of death in more economically developed countries like the United States.[1] From the numerous drugs clinically used to treat cancer, cisplatin[2] plays a key role in fighting several types of cancer.[3] The remarkable properties of cisplatin instigated a new area of anticancer chemical research based on platinum-containing compounds.[4] However, platinum drugs suffer from some severe drawbacks: (i) they are inefficient against platinum-resistant tumors,[5] and (ii) they are usually highly toxic, causing many undesirable side effects.[6] Therefore, the search for more efficient and less toxic, new anticancer agents is relentless.[7]

In that context, the use of other metal ions to cope with platinum resistance is a strategy that is increasingly being exploited.[8,9] For instance, some ruthenium compounds have shown promising activities,[10,11] particularly organoruthenium complexes.[12,13] For example, (η^6-arene)ruthenium complexes, i.e., ruthenium half-sandwich complexes, have been developed that exhibit interesting anticancer features.[14] In this category of Ru compounds, those belonging to the RAPTA family are certainly the most known ones,[15] thanks to their attractive pharmacological properties.[16,17] After the discovery of the interesting pH-dependent DNA-damaging properties of RAPTA-C (i.e., [Ru(η^6-*p*-cymene)Cl_2(pta)], with pta = 1,3,5-triaza-7-phosphatricyclo-[3.3.1.1]decane; see Scheme 1),[18] a number of ruthenium compounds derived from it have been developed,[15] including analogues for which the pta ligand has been replaced with another phosphane.[19]

In the present study, new piano-stool ruthenium(II) complexes have been designed, which contain a 1-pyrene-containing monophosphane ligand, the other two P-substituents being methyl or/and phenyl groups (Scheme 1). Two different η^6-arene ligands have also been used, namely, η^6-*p*-cymene and η^6-methyl benzoate, with the objective to

Received: September 7, 2018

DOI: 10.1021/acs.inorgchem.8b02541
Inorg. Chem. XXXX, XXX, XXX–XXX

Scheme 1. Representations of the Structure of RAPTA-C (left) and That of the Analogues 1−6 Designed and Prepared in the Present Study

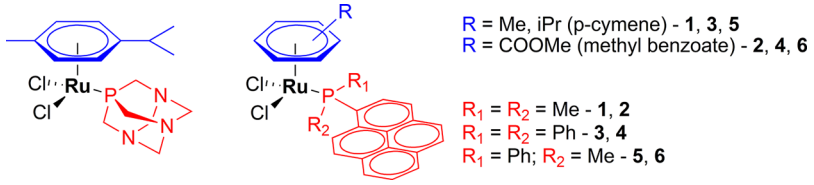

Scheme 2. Synthetic Procedure for the Preparation of the 1-Pyrenylphosphane Ligands L1−L3

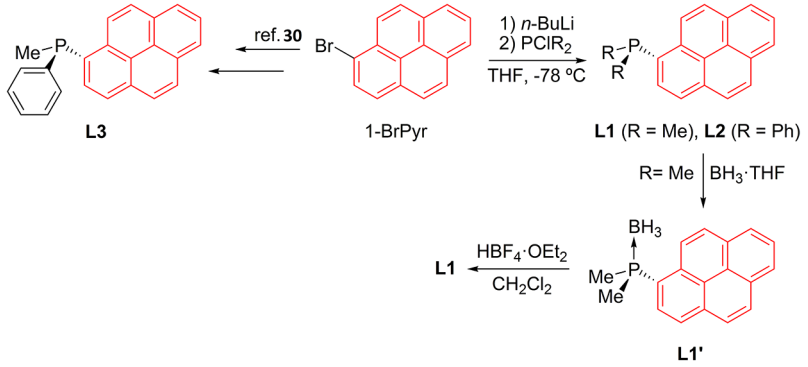

Scheme 3. Synthetic Pathways (Procedures A and B) Used for the Preparation of the Piano-Stool Ruthenium Complexes

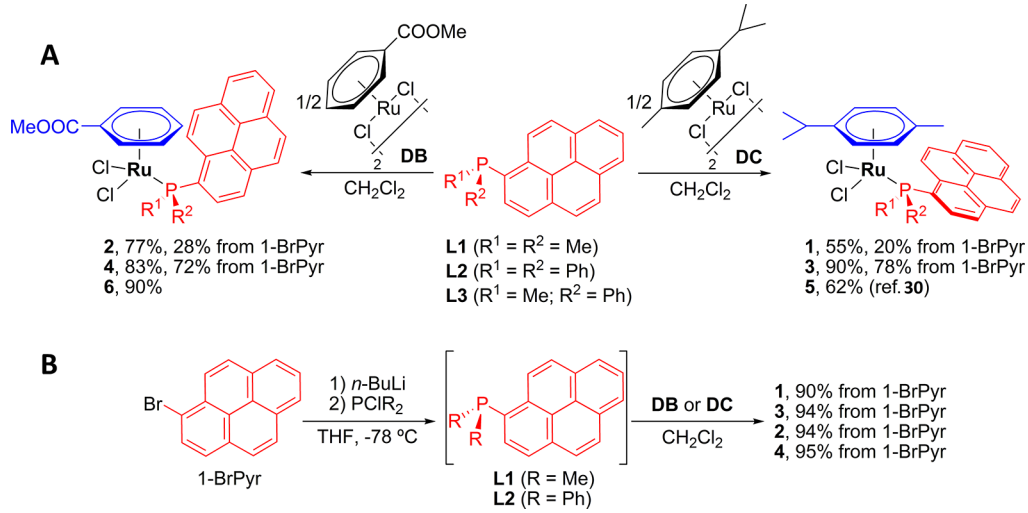

investigate the influence of the electronic character of the aryl ring on the biological activities of the corresponding complexes; it is indeed known that an electron-poor arene such as a methyl benzoate is more labile than an electron-rich one like *p*-cymene,[20] and favors the hydrolysis of Ru−Cl bonds.[21]

The choice of the pyrenyl substituent on the phosphane ligand is based on the chemical nature of its structure. Pyrene is the smallest peri-fused polycyclic arene with high symmetry.[22] The planar structure of this aromatic molecule (following Clar sextet rule[23]) is crucial as it may allow the occurrence of $\pi-\pi$ stacking interactions, for instance, between DNA base pairs.[24,25] The other P-substituents, namely, methyl or phenyl, have been elected to examine the effect of an alkyl or an aryl group on the biological activity of the resultant Ru half-sandwich complex.

Thus, three monophosphane ligands have been prepared, namely, dimethyl(1-pyrenyl)phosphane (**L1**), diphenyl(1-pyrenyl)phosphane (**L2**), and (*S*)-methylphenyl(1-pyrenyl)-phosphane (*S*-**L3**) (Scheme S1). Subsequently, piano-stool ruthenium(II) chlorido complexes have been synthesized from these three P-ligands and using η^6-*p*-cymene and η^6-methyl benzoate; hence, six metal complexes were obtained (Schemes 1 and S1; compounds **1−6**). The evaluation of their in vitro biological properties (interaction with DNA, cytotoxicity, and cell-cycle studies) revealed drastic differences ascribed to their structural variations.

RESULTS AND DISCUSSION

Preparation of the Ligands and the Half-Sandwich Ruthenium(II) Arene Complexes. Phosphane Ligands. Dimethyl(1-pyrenyl)phosphane (**L1**), diphenyl(1-pyrenyl)-phosphane (**L2**), and (*S*)-methylphenyl(1-pyrenyl)phosphane (*S*-**L3**) were prepared using usual synthetic procedures. The synthesis of achiral 1-pyrenyl phosphanes **L1** and **L2** was

DOI: 10.1021/acs.inorgchem.8b02541
Inorg. Chem. XXXX, XXX, XXX−XXX

carried out by metalation of commercially available 1-bromopyrene (1-BrPyr) with *n*-BuLi, and subsequent reaction of the formed 1-pyrenyllithium solution with the appropriate chlorophosphane $PClR_2$ (Scheme 2).

Ligand **L2** was previously reported by Yip and co-workers,[26] who used a similar synthetic procedure. In contrast, ligand **L1** is herein described for the first time. Following the typical pathway, it was found that **L1** is prone to oxidation and therefore could not be purified. Accordingly, crude **L1** was treated with BH_3·THF to generate the corresponding air-stable borane **L1′** (Scheme 2), which could be purified by column chromatography, although with a moderate yield of 41%. Subsequent standard deboronation of **L1′** with HBF_4·OEt_2[27] yielded pure **L1** as an air-sensitive semisolid compound, whose highly shielded $^{31}P\{^1H\}$ chemical shift of −59.6 ppm is in line with those of other reported aryldimethylphosphanes.[28,29] Overall, ligand **L1** was obtained with a yield of 36% yield from 1-BrPyr (1-bromopyrene). Finally, the preparation of the *P*-stereogenic phosphane (*S*)-**L3** was carried out applying the Jugé-Stephan methodology, employing (−)-ephedrine as chiral auxiliary, as previously reported by some of us.[30]

Ruthenium η^6-Arene Complexes. The synthesis of the different ruthenium complexes was initially performed by reaction of the corresponding phosphane ligand with the appropriate ruthenium dimers, i.e., $[RuCl(\mu\text{-}Cl)(\eta^6\text{-}p\text{-cymene})]_2$ (**DC**) or $[RuCl(\mu\text{-}Cl)(\eta^6\text{-methyl benzoate})]_2$ (**DB**) (Procedure **A**, Scheme 3).[31−33]

Using this procedure, the desired complexes **1**, **3**, **5** and **2**, **4**, **6** were obtained as brown or reddish solids; these compounds are reasonably stable in the solid state but are somewhat unstable in solution, especially in the presence of light. Complex **5** was previously reported by some of us.[30]

Although Procedure **A** allows the Ru compounds, to be produced, it requires the use of the isolated phosphane ligands, which results in low yields (probably due to partial ligand oxidation); for instance, ligand **L1** had to be purified via its phosphane-borane derivative **L1′**, which was obtained in low yield (see above). For these reasons, an alternative one-pot method (Procedure **B**; Scheme 3) was developed for the preparation of the complexes containing ligand **L1** or **L2**. After the lithiation and phosphination of 1-BrPyr in THF, the solvent was removed and replaced by CH_2Cl_2, providing a suspension of the phosphane and the lithium salts. Dimer **DB** or **DC** was directly added to this mixture, producing the desired ruthenium complexes in high yields (90−95%). These organoruthenium compounds were characterized by common techniques, which confirmed their identity (see Experimental Section for details). It should be noted that, in some cases, broad ^1H NMR signals were observed, especially for the protons of the coordinated arene ring, possibly due to its slow rotation resulting from the bulkiness of the phosphane ligand.

Description of the Crystal Structures of Ru Compounds 1, 2, and 4. Crystals of compounds **1**, **2**, and **4**, suitable for X-ray diffraction measurements, could be obtained (see Experimental Section).

Compounds **1** and **2** crystallize in the monoclinic space group $P2_1/c$, and compound **4** crystallizes in the triclinic space group $P\bar{1}$ (Table S1). The solid-state structures of the Ru(II)-arene compounds are shown in Figure 1, and selected bond lengths and angles are listed in Table 1. The three organoruthenium complexes show the typical pseudo-octahedral "three-legged piano stool" geometry around the metal center.

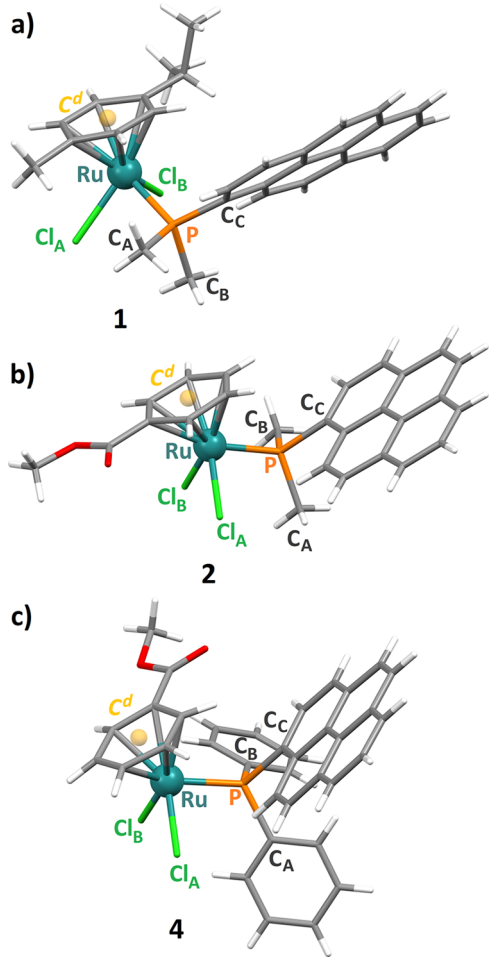

Figure 1. Representation of the crystal structures of (a) $[RuCl_2(\eta^6\text{-}p\text{-cymene})$**L1**$]$ (**1**), (b) $[RuCl_2(\eta^6\text{-methyl benzoate})$**L1**$]$ (**2**), and (c) $[RuCl_2(\eta^6\text{-methyl benzoate})$**L2**$]$ (**4**).

Table 1. Selected Bond Lengths (Å) and Angles (deg) for Compounds 1, 2, and 4[a]

	Bond Distances (Å)			
	Ru−P	$Ru-Cl_A$	$Ru-Cl_B$	$Ru-C_d$
Complex **1**	2.331(1)	2.422(1)	2.413(1)	1.690(1)
Complex **2**	2.326(2)	2.390(2)	2.390(1)	1.682(2)
Complex **4**	2.387(1)	2.397(1)	2.441(1)	1.704(1)
	Bond Angles (deg)			
	$Cl_A-Ru-Cl_B$	Cl_A-Ru-P	Cl_B-Ru-P	C_d-Ru-P
Complex **1**	86.4(1)	82.7(1)	90.6(1)	127.5(1)
Complex **2**	85.6(1)	83.8(1)	88.2(2)	126.1(1)
Complex **4**	87.1(1)	90.0(1)	88.3(1)	130.8(1)
	$Ru-P-C_A$	$Ru-P-C_B$	$Ru-P-C_C$	C_A-P-C_B
Complex **1**	111.2(2)	117.5(2)	114.9(2)	99.8(2)
Complex **2**	115.0(2)	110.1(2)	117.4(2)	104.3(3)
Complex **4**	118.4(1)	114.2(1)	113.5(1)	101.7(1)

[a] Cl_A, Cl_B, C_C, and C_d are defined in Figure 1.

The distance between the metal ion and the centroid of the η^6-arene ring, i.e., $Ru-C_d$, is 1.690(1), 1.682(2), and 1.704(1) Å for **1**, **2**, and **4**, respectively. The three legs of the stool are formed by two σ-bonded chlorides, namely, Cl_A and Cl_B (at normal distances, *viz.* in the range 2.39−2.44 Å; Table 1), and the phosphane ligand, with Ru−P bond lengths of 2.331(1)

DOI: 10.1021/acs.inorgchem.8b02541
Inorg. Chem. XXXX, XXX, XXX−XXX

(**1**), 2.326(2) (**2**), and 2.387(1) (**4**) Å. The slightly longer Ru−Cl_B distance observed for **4** may be due to steric hindrance of the phenyl substituents of **L2**; in fact, Cl_B is located between the two phenyl rings (Figure 1c). Similarly, the longer Ru−P bond length in **4** probably arises from the greater steric bulk of ligand **L2**.

The coordination angles, for instance, the P−Ru−Cl and Cl_A−Ru−Cl_B angles (Table 1), are in normal ranges for such Ru(II)-arene compounds.[34,35] Some slight angle differences are noticed for the tetrahedral phosphorus atom of the coordinated phosphane ligand (Ru, C_A, C_B, and C_C; Figure 1 and Table 1). These variations are most likely due to the distinct bulkiness of the respective η^6-arene moieties. For instance, constraints due to the larger *p*-cymene ligand in **1** (compared with η^6-methyl benzoate; compound **2**) appear to force the methyl−phosphorus−methyl angle to be below 100° (C_A−P−C_B = 99.8(2)° in **1** and C_A−P−C_B = 104.3(3)° in **2**; Table 1). The average of the R−P−R′ angles (i.e., C_A−P−C_B, C_B−P−C_C, and C_C−P−C_A; see Figure 1) for ligand **L1** in **1** is 103.8°, while the value is 104.3° in **2** (Table S2). For **4**, the average of the apex R−P−R′ angles is smaller, viz. 103.0° (Table S2), suggesting that **L2** induces more sterical constraints than **L1**; this is further corroborated by the angle C_d−Ru−P of 130.8° observed for **4**, which is clearly greater than those of **1** and **2** (Table 1).

While the crystal packing of **1** does not show any remarkable features, that of **2** presents some intermolecular supramolecular contacts. The lower steric hindrance of the η^6-methyl benzoate ring (compared to *p*-cymene; compound **1**) allows the occurrence $\pi-\pi$ interactions between pyrene groups from neighboring Ru molecules, the shortest contact distance being C5···C15e = 3.162(7) Å (symmetry operation; e = 1 − *x*, 1/2 + *y*, 1/2 − *z*) (Figure S1). These supramolecular bonds generate a one-dimensional (1D) chain along the crystallographic *b* axis. The crystal packing of **4** shows the formation of head-to-tail supramolecular dimers via $\pi-\pi$ stacking between the pyrenes and methyl benzoate arenes, the shortest contact distance being of 3.246(4) Å (C8···C 4f; symmetry operation: *f* = −*x*, 2 − *y*, −*z*) (Figure S2). The dimers of **4** are further involved in $\pi-\pi$ interactions with two adjacent dimers through phenyl rings of the phosphane ligand **L2** (shortest distance being C35···C35h = 3.280(4) Å; symmetry operation: h = −*x*, 1 − *y*, 1 − *z*); these contacts give rise to the generation of a supramolecular chain (Figure S2).

Interaction with DNA. The potential binding of compounds **1**−**6** to DNA was then examined using various common techniques. The DNA-binding properties of the six ruthenium compounds were first investigated using agarose gel electrophoresis.[36,37] Figure 2 shows the electrophoretic data obtained for **1**, which are representative of the other ruthenium compounds examined in the present study, namely, compounds **2**−**6** (Figure S3). In the case of compound **1**, no changes are noticed (compared with the original DNA; lane 1), even when its concentration is increased (Figure 2, lanes 4−7). Actually, DNA forms I and II are observed with the same electrophoretic mobilities as those of the original DNA for all ruthenium compounds (see Figures 2 and S3); it thus appears that **1**−**6** are not capable of (covalently) binding/interacting with the biomolecule.

Next, the potential interaction **1**−**6** with DNA was assessed by fluorescence-dye displacement studies, using the intercalating agent ethidium bromide (EB).[38] The results achieved with compounds **1**−**6**, using [DNA]/[complex] ratios of 15, 7.5, 5, 2.5, 1.67, 1.25, 1, 0.75, and 0.6, are illustrated in Figure S4. No decrease of the fluorescence of the [EB-DNA] complex is detected; hence, EB is not displaced by the ruthenium compounds, suggesting that they are not (strongly) interacting with the duplex, as already observed by gel electrophoresis (see above). Actually, a small increase of the fluorescence is noticed upon increasing the complex concentration (see Figure S4), which may arise from a slight unwinding of the double helix that improves the intercalation of EB; Cuniberti and Guenza indeed have shown that environmental changes altering/modifying the secondary structure of DNA can enhance the fluorescence (improved quantum yield) of the [EB-DNA] system.[39] Thus, most likely, high concentrations of Ru compounds promote the occurrence of some interaction with DNA (for instance, via electrostatic or hydrogen-bonding contacts with the phosphate backbone), which, in turn, gives rise to a better intercalation of EB, accompanied by an enhancement of the fluorescence.

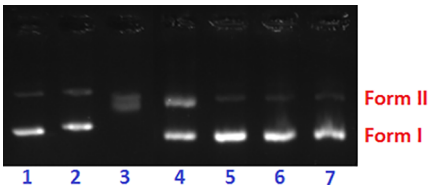

Figure 2. Agarose gel electrophoresis image for pBR322 DNA ($[DNA]_{bp}$ = 15 μM) incubated for 24 h at 37 °C with increasing concentrations (6.25−50 μM) of compound **1** in cacodylate buffer. Lane 1: native plasmid DNA; lane 2: DNA + 0.5 equiv of cisplatin; lane 3: DNA + 1 equiv of cisplatin; lane 4: DNA + 0.42 equiv **1**; lane 5: DNA + 0.83 equiv **1**; lane 6: DNA + 1.67 equiv **1**; lane 7: DNA + 3.33 equiv **1**.

In Vitro Cell-Viability Studies. The ability of compounds **1**−**6** to inhibit cell growth was first evaluated against four cancer cell lines, namely, the human lung adenocarcinoma (A549), melanoma (A375), colorectal adenocarcinoma (SW620), and breast adenocarcinoma (MCF7), which are representative of some of the most common cancers. A nontumorigenic epithelial breast cell line, viz. MCF10A, was also tested for comparison. Quarter-, half-, and three-quarter-maximal inhibitory concentrations were determined for all compounds after an incubation time of 24 h with each cell line (Tables S3−S7). The IC_{50} values (in μM) are listed in Table 2. In general, the organoruthenium complexes show significant cytotoxic activities against most of the cell lines investigated (IC_{50}'s in the low micromolar range). It is important to stress that structure−activity relationships (SARs) are observed. Indeed, compounds **1** and **2** only differ by their η^6-arene moiety, being η^6-*p*-cymene for **1** and η^6-methyl benzoate for **2** (Scheme 3).

Compound **2** is significantly more active than **1** in all cell lines tested (Table 2); actually, **2** is up to 4 times more cytotoxic than **1** (see Table 2, A375 cell line: 2.19 versus 8.99 μM for the corresponding IC_{50} values). This clear difference may be due to the known better dissociation of the η^6-benzoate group compared with that of the η^6-*p*-cymene one.[20] Furthermore, it has also been shown that a ruthenium half-sandwich complex containing a η^6-ethyl benzoate ring was much more easily hydrolyzed than its η^6-*p*-cymene counterpart, as reflected by the respective half-life times $t_{1/2}$ of 14.5 and 92.3 min.[21] Two effects, namely, arene dissociation and hydrolysis (which may occur simultaneously), can therefore

DOI: 10.1021/acs.inorgchem.8b02541
Inorg. Chem. XXXX, XXX, XXX−XXX

Table 2. Half-Maximal Inhibitory Concentrations[a] (IC_{50}, μM) of Compounds 1−6 for the A549 (Lung Adenocarcinoma), A375 (Melanoma), SW620 (Colorectal Adenocarcinoma), MCF7 (Breast Carcinoma) and MCF10A (Non-Tumorigenic Epithelial Breast) Human Cell Lines, after Incubation of 24 h[b]

	cell line				
compound	A549	A375	SW620	MCF7	MCF10A
1	17.16 ± 0.53	8.99 ± 0.07	6.46 ± 0.78	9.74 ± 0.13	6.88 ± 0.31
2	**5.01** ± 0.59	**2.19** ± 0.02	**1.93** ± 0.09	**5.05** ± 1.56	**5.53** ± 0.95
3	74.73 ± 2.31	25.01 ± 1.83	28.53 ± 0.93	36.15 ± 5.22	34.69 ± 3.63
4	**23.24** ± 0.85	**15.49** ± 1.70	**8.17** ± 0.75	**18.84** ± 0.36	**16.83** ± 0.29
5	**8.74** ± 1.01	**4.21** ± 0.41	3.14 ± 0.40	**5.40** ± 1.01	**4.31** ± 0.37
6	10.02 ± 1.59	5.19 ± 0.72	**2.70** ± 0.20	7.08 ± 0.95	8.95 ± 0.59

[a]The results are expressed as mean values ± SD out of three independent experiments. [b]The lowest IC_{50} for each series (namely, **1**−**2**, **3**−**4**, and **5**−**6**) are shown in bold.

explain the distinct biological activity of **1** and **2**. DNA interaction studies (see above) suggested that compounds **1**−**6** are not targeting the genetic material. Thus, the activation of **2** through the loss of the arene ligand and/or hydrolysis of the chloride ions most likely affects other cellular component(s), leading to cell death. Finally, it can also be mentioned here that it has been described that the "η^6-ethyl benzoate equivalent" of RAPTA-C, i.e., RAPTA-CO_2Et ([Ru(η^6-ethyl benzoate)-Cl_2(pta)], was toxic against epithelial HBL-100 cells, whereas RAPTA-C was not, thus again showing the "beneficial" effect of the benzoate ring on the activity.[17] To verify further this hypothesis, the stability of **2** in DMSO (viz. the solvent used to prepare the stock solutions of the complexes for the biological studies; see Experimental Section) was examined by ^{1}H NMR. The corresponding NMR spectra after up to 64 h are shown in Figure S5. The release of free methyl benzoate over time is clearly observed; traces of the aromatic compound are already discerned at time zero. After 64 h, quite a significant amount of methyl benzoate is detected. In contrast, the same studies carried out with **1** under the same experimental conditions revealed the presence of only traces of *p*-cymene, even after 72 h (Figure S6). These preliminary studies hence indicate that the η^6-ethyl benzoate ring is a better "leaving group" than the η^6-*p*-cymene one, therefore corroborating our supposition. More (mechanistic) in-depth studies are obviously required to elucidate the nature of the species generated upon release of the η^6-arene ligand.

This tendency is observed as well with compounds **3** and **4** (Table 2); indeed, **4** is 1.6−3.5 times more cytotoxic than **3** in all cell lines tested. Comparison of the IC_{50} values of **1** and **3**, and of **2** and **4** reveals that replacement of ligand **L1** (compounds **1** and **3**) by **L2** (compounds **2** and **4**) gives rise to a significant decrease of the cytotoxic activity; for instance, **3** is up to 5 times less toxic than **1**, and **4** is up to 7 times less efficient than **2** (Table 2). These differences may be explained by the distinct bulkiness of **L1** and **L2**; the higher steric hindrance of **L2** (compared with that of **L1**) may reduce the binding aptitude of the corresponding complexes toward their cellular target(s) (the metal center being sterically more protected).

Compounds **5** and **6**, containing the chiral ligand (*S*)-**L3** (having a methyl and a phenyl *P*-substituents, in addition to the 1-pyrenyl group), exhibit cytotoxic behaviors that are (logically) in-between those of the dimethyl-containing **L1** (**1** and **2**) and diphenyl-containing **L2** (**3** and **4**) complexes (Table 2). However, the activities of **5** and **6** are close to those of **1** and **2** (Table 2); therefore, the sole replacement of one of the phenyl groups of ligand **L2** by a methyl, i.e., ligand (*S*)-**L3**, is sufficient to enhance the toxicity of the corresponding ruthenium compounds by a factor of 1.9 up to 9.1 (Table 2). It is important to notice that for this methyl/phenyl series, the cytotoxicities of **5** and **6** are similar (in marked contrast to the pairs **1**−**2** and **3**−**4**); moreover, the η^6-*p*-cymene-containing compound **5** is, in most cases, slightly more active than its η^6-methyl benzoate counterpart, viz. compound **6** (**6** is only more cytotoxic than **5** against the colorectal cell line SW620; Table 2). Thus, the choice/influence of the η^6-arene and PR_3 ligands seems to be quite subtle; an apparently insignificant/minor structural modification of the metal compound can give rise to a notable change of its biological activity. Accordingly, the properties of such ruthenium derivatives may be fine-tuned (thanks to the high versatility of the η^6-arene- and PR_3-type ligands).

The selectivity indexes (SIs) for compounds **1**−**6** were determined with the nontumorigenic epithelial breast cell line MCF10A and the breast adenocarcinoma cell line MCF7. The SI is expressed as the IC_{50} of the compound in the normal cell line divided by IC_{50} of the compound in the cancer cell line. The calculated data are listed in Table 3. The SI values vary from 0.71 to 1.26; hence, the selectivity of the compounds toward the breast cancer cells is poor. Only compound **6** is slightly less toxic to healthy cells (Table 3).

Table 3. Selectivity Index (SI) = IC_{50} MCF10A (Non-Cancerous Cell Line)/IC_{50} MCF7 (Cancerous Cell Line) of Compounds 1−6

1	2	3	4	5	6
0.71	1.10	0.96	0.89	0.80	**1.26**

Cell-Cycle and Apoptosis Studies. Cell-cycle analyses by quantitation of DNA content using flow cytometry were then performed with A375 cells incubated for 24 h with compounds **1**−**6**. Three control experiments were also carried out, namely, (i) without any added compound, (ii) in the presence of cisplatin, and (iii) in the presence of staurosporine, an inhibitor of protein kinases (that is used to induce apoptosis). The corresponding results as the percentages of cells in the G_0/G_1, S, and G_2/M phases of the cell cycle are listed in Table 4. As expected, cisplatin stops the cell cycle at the S and G_2/M phases (Table 4); indeed, it is well-known that the main effects of cisplatin are S-phase and G_2-phase arrest.[40−42] Staurosporine induces a cell-cycle arrest at the G_2/M phase. It is known that staurosporine inhibits the expression of major cell-cycle proteins at the G_2/M checkpoint, giving rise to apoptosis.[43] From compounds **1**−**6**, only **2** and **4** appear to alter the cell

DOI: 10.1021/acs.inorgchem.8b02541
Inorg. Chem. XXXX, XXX, XXX−XXX

Table 4. Cell-Cycle Analysis[a]

compound	G_0/G_1 phase	S phase	G_2/M phase
control[b]	56.3 ± 3.3	16.0 ± 1.2	27.7 ± 3.4
cisplatin[c]	26.1 ± 3.4	**31.1 ± 3.4**	**42.8 ± 5.1**
staurosporine[b]	28.0 ± 4.2	17.3 ± 1.5	**54.6 ± 4.5**
1[b]	58.4 ± 2.4	19.6 ± 2.2	22.0 ± 2.1
2[b]	30.8 ± 3.4	**25.1 ± 1.6**	**44.1 ± 4.6**
3[b]	62.1 ± 3.3	13.3 ± 2.9	24.6 ± 1.1
4[b]	46.7 ± 2.5	16.6 ± 0.7	**36.7 ± 2.9**
5[b]	51.8 ± 1.7	21.3 ± 4.3	26.9 ± 2.6
6[b]	52.0 ± 5.6	17.8 ± 2.6	30.2 ± 3.6

[a]Percentage of A375 (melanoma) cells with Gap 0 (G_0)/ Gap 1 (G_1), DNA synthesis (S), and Gap 2 (G_2)/mitosis (M) phase DNA content, determined by flow cytometry after 24 h incubation (without any added compound but with 1% DMSO), 48 h incubation with cisplatin, 24 h incubation with staurosporine, and 24 h incubation with **1**–**6**. The data given are means ± SD of three independent experiments. [b]Incubation of 24 h. [c]Incubation of 48 h.

cycle of A375 cells (Table 4). Remarkably, compound **2** seems to block the cell cycle at the S and G_2/M phases, like cisplatin (Table 4). Interestingly, **2** is the most active compound of the series described in the present study (Table 3); it should however be reminded that the mechanism of action of **2** is apparently different from that of cisplatin (the cellular target of **2** most likely is not DNA; see above). Compound **4** produces some G_2/M arrest, while **1**, **3**, **5**, and **6** have no effect on the cell cycle (Table 4). Clearly, the cellular target of these organoruthenium(II) complexes is not the genetic material.

Next, the quantitative analysis of live cells, early and late apoptosis and cell death was carried out using the Muse annexin V and dead cell assay to assess the potential ability of **1**–**6** to induce A375-cell apoptosis. The experiments were performed using an incubation time of 24 h, and complex concentrations corresponding to the respective IC_{50} value of **1**–**6** for this cell line (at this incubation time; see Table 2). Controls with 5 μM cisplatin and 200 nM staurosporine were also done for comparison purposes. The results, shown in Table 5, indicate that all compounds are capable of inducing apoptosis, but with distinct orders of magnitude. The ruthenium(II) complexes can be divided into two groups, namely, those causing moderate apoptosis, i.e., **2** and **3**, and those inducing apoptosis, i.e., **1**, **4**, **5**, and **6** (Table 5).

The activity of **1** and **6** is comparable with that of cisplatin, while that of **4** and **5** is closer to the behavior observed for staurosporine; using complex concentrations corresponding to their respective IC_{50} values, **4** and **5** give rise to analogous apoptosis. Since **5** is 2.5–4 times more cytotoxic than **4** (see Tables 2 and 5), the apoptosis data suggest that their mechanism of action is different. Remarkably, compound **2**, which exhibits the best IC_{50} values (against all tested cell lines; see Table 2) and is able to stop the cell cycle at the S and G_2/M phases (like cisplatin; see Table 4), is the least efficient complex regarding the induction of apoptosis; hence, its efficacy is clearly due to its capacity to block the cell cycle. Actually, the behavior of **2** is similar to that of **3**, which is the least cytotoxic compound of the series (see Tables 2 and 5).

In summary, the cell-cycle and apoptosis studies described above clearly suggest that, even though **1**–**6** are structurally close to each other, they do not act with the same mechanism of action; indeed, the (apparently) slight structural variations among them give rise to important changes of their biological activity toward A375 cells. More in-depth biological investigations are necessary to determine the specific way in which each compound affects the cells.

Biological Activity against Neuroblastoma Cells. Neuroblastoma is the most common embryonic malignancy of early childhood whose prognosis is very poor, especially for infants diagnosed between birth and 18 months of age.[44] This pediatric disease presents a high metastatic rate that ultimately affects the liver, bone marrow, and skin, as well as several other organs.[45] 7-Ethyl-10-hydroxy-camptothecin, also known as **SN-38**, is one of the current antineoplastic drugs that is used clinically against neuroblastoma. **SN-38** is the active metabolite of irinotecan, viz. (4*S*)-4,11-diethyl-4-hydroxy-3,14-dioxo-3,4,12,14-tetrahydro-1*H*-pyrano[3′,4′:6,7]indolizino[1,2-*b*]-quinolin-9-yl 1,4′-bipiperidine-1′-carboxylate (Figure S5), which is also active against this cancer;[46] however, **SN-38**, generated through hydrolysis of irinotecan, is 1000 times more active than the parent compound.[47] It should be pointed out that **SN-38**, which acts as an inhibitor of DNA topoisomerase I, exhibits a high toxicity and solubility issues;[48] therefore, the development of more efficient drugs with increased tolerance is of paramount importance for the treatment of this lethal childhood cancer.

The efficient **L1**-containing compounds **1** and **2** (see above) were hence tested against two human neuroblastoma cell lines, namely, SK-N-BE(2) and CHLA-90. Both cell lines are from the same disease stage and postchemotherapy, but SK-N-BE(2) presents MYCN amplification, whereas CHLA-90 does not. The cytotoxic activities of **1** and **2** were compared with

Table 5. Apoptosis Analysis[a]

compound	live cells	early apoptotic cells	late apoptotic cells	total apoptotic cells	dead cells (other)
control	95.1 ± 1.0	2.6 ± 1.0	2.0 ± 1.3	4.6 ± 0.8	0.2 ± 0.3
cisplatin	62.8 ± 9.4	3.7 ± 2.9	33.1 ± 6.9	**36.7 ± 9.7**	0.5 ± 0.3
staurosporine	51.2 ± 1.7	23.6 ± 2.8	25.1 ± 3.2	**48.6 ± 1.7**	0.2 ± 0.1
1	59.3 ± 9.8	2.6 ± 1.5	33.5 ± 5.7	**36.1 ± 7.1**	**4.6 ± 2.8**
2	80.9 ± 3.1	6.7 ± 4.4	12.0 ± 4.0	**18.8 ± 3.5**	0.3 ± 0.4
3	78.5 ± 1.8	12.2 ± 6.5	8.6 ± 4.2	**20.8 ± 2.5**	0.7 ± 0.7
4	52.0 ± 5.6	9.2 ± 3.2	32.5 ± 5.2	**41.8 ± 2.8**	**6.3 ± 3.4**
5	59.8 ± 11.2	22.6 ± 3.9	17.5 ± 7.4	**40.1 ± 11.2**	0.1 ± 0.1
6	66.8 ± 11.2	18.6 ± 4.6	14.5 ± 6.6	**33.1 ± 11.2**	0.1 ± 0.1

[a]Percentage of A375 (melanoma) live, early apoptotic, late apoptotic and dead cells after 24 h incubation with IC_{50} concentrations of **1**–**6**. Control experiments were carried out without any added compound (24 h incubation and containing 1% DMSO), 5 μM cisplatin (48 h incubation), and 200 nM staurosporine (24 h incubation). The data given are means ± SD of three independent experiments.

DOI: 10.1021/acs.inorgchem.8b02541
Inorg. Chem. XXXX, XXX, XXX–XXX

those of the reference compound **SN-38**; the corresponding IC_{50} values are listed in Table 6.

Table 6. IC_{50} Values (μM) of Compounds 1 and 2, and the Reference Drug SN-38 for the Neuroblastoma Cell Lines SK-N-BE(2) and CHLA-90, Determined after an Incubation Time of 24 h[a]

compound	SK-N-BE(2)	CHLA-90
1	3.2 ± 0.4	3.0 ± 0.1
2	0.50 ± 0.02	0.40 ± 0.05
SN-38	7.6 ± 0.6	13.0 ± 0.8

[a]The data shown are means ± SD of three independent experiments.

Both ruthenium(II) complexes are more effective than **SN-38**; compound **2** is particularly active, as evidenced by its IC_{50} values in the nanomolar range (Table 6). It can be noted that, again, the η^6-methyl benzoate derivative, i.e., **2**, is significantly more efficient than η^6-*p*-cymene-containing **1** (6.4 and 7.5 times more active against SK-N-BE(2) and CHLA-90 cells, respectively; Table 6).

The effect of **1** and **2** on cell migration was next investigated using the same two neuroblastoma cell lines (SK-N-BE(2) and CHLA-90). For this study, the wound-healing assay was used. This assay is a standard in vitro technique to probe collective cell migration in two dimensions. It consists of removing cells from an area through mechanical, thermal, or chemical damage, creating a "wound" (i.e., a cell-free zone) in a confluent monolayer. Afterward, images were regularly taken with an inverted-phase contrast microscope and the area closure (viz. "wound healing") was quantified (see Experimental Section for details). It should be stressed here that mitomycin C was used in all experiments. Mitomycin C is an inhibitor of cell division (proliferation); its utilization therefore ensures that the closure of the wound is solely due to cell migration and not to cell division. The calculated areas (quantification of the closure; see Experimental Section) were plotted against time, providing two parameters, namely, the time required to close half of the wound, i.e., $t_{1/2}$ (hours) and the migration velocity (or cell-migration rate), namely, $V_{migration}$ (μm h^{-1}). The data obtained for SK-N-BE(2) and CHLA-90 cells in the presence of **1** and **2** are given in Table 7. The corresponding microscopy images are shown in Figures S8 and S9 for the SK-N-BE(2) and CHLA-90 cells, respectively.

Table 7. Calculated Times to Reduce by Half the Wound Area ($t_{1/2}$; h) and Cell-Migration Rates ($V_{migration}$; μm h^{-1}) for 1 and 2 with the Two Neuroblastoma Cell Lines SK-N-BE(2) and CHLA-90[a]

	SK-N-BE(2)		CHLA-90	
	$t_{1/2}$ (h)	$V_{migration}$ (μm h^{-1})	$t_{1/2}$ (h)	$V_{migration}$ (μm h^{-1})
control[b]	23.1 ± 4.4	7.8 ± 0.0	18.6 ± 4.3	7.8 ± 0.5
1	27.8 ± 0.5	7.6 ± 0.3	17.3 ± 2.0	8.9 ± 0.5
2	**37.2** ± 3.7	**3.0** ± 0.3	21.1 ± 5.9	8.0 ± 0.9

[a]The data for the ruthenium compounds are compared with those of the control (cells without added compound). All data shown are means ± SD of three independent experiments. In all cases, cell division (proliferation) was inhibited using mitomycin C. [b]Without added compound.

For SK-N-BE(2) cells, compound **1** has almost no effect on their migratory capacity. However, compound **2** significantly decreases the ability of the cells to migrate as 33% more time is required to reduce half the wound area (compared with the control; Table 7). In the presence of **2**, SK-N-BE(2) cells are more than 60% slower compared with the compound-free ones (Table 7). In the case of the CHLA-90 cells, both compounds **1** and **2** do not affect their migration rate.

In summary, the present preliminary studies revealed that the migration of SK-N-BE(2) cells was markedly inhibited when the cells were pretreated with **2**; hence, more in-depth biological investigations are definitively required to assess the potential "antimetastatic properties" of **2** (with certain cell line(s)).

CONCLUSIONS

The biological (cytotoxic) activities of a series of ruthenium half-sandwich complexes, bearing a 1-pyrenyl-containing phosphane ligand, have been assessed against various human cell lines. The data achieved revealed that both the nature of the η^6-arene and PR^1R^2(1-pyrenyl) ligands of the compounds with formula $[Ru(\eta^6\text{-arene})Cl_2(PR^1R^2(1\text{-pyrenyl}))]$ are important regarding their respective biological behavior. Indeed, the compounds with a methyl benzoate η^6-ring are generally more efficient than the *p*-cymene ones. The bulkiness of the P-ligand also appears to be a key factor as the Ru complexes from the $P(Me)_2$(1-pyrenyl) phosphane are significantly more effective than those containing the $P(Ph)_2$(1-pyrenyl) phosphane. Replacement of one of the phenyl substituents of $P(Ph)_2$(1-pyrenyl) by a methyl group, giving the "mixed" ligand P(Me)(Ph)(1-pyrenyl), logically generate metal compounds with intermediate cytotoxicities (but close to those of the $[P(Me)_2$(1-pyrenyl)]-containing complexes). All compounds are capable of inducing apoptosis (with various efficacies), and the most active Ru complex, combining the two beneficial ligands (namely, methyl benzoate and $P(Me)_2$(1-pyrenyl)), arrests the cell cycle at the G_2/M and S phases, like cisplatin. However, this piano-stool compound, like all the other complexes of the series, apparently does not target DNA (in contrast to cisplatin), even though the 1-pyrenyl moiety was expected to promote DNA-intercalating properties. Other cellular target(s) is(are) obviously affected by this family of compounds, which has(ve) to be determined. Finally, the best complex, namely, $[RuCl_2(\eta^6\text{-methyl benzoate})(PMe_2(1\text{-pyrenyl}))]$ (**2**), shows the ability to act as a cell-migration inhibitor for a certain cell line.

The present study clearly illustrates the high potential of such versatile $[RuCl_2(\eta^6\text{-arene})(PR^1R^2R^3)]$ compounds as possible antineoplastic agents. Clearly, the activity of such complexes can be (fine-)tuned through:

(i) Their η^6-arene ligand. It has been observed that the aryl ring with an electron-withdrawing substituent, i.e., methyl benzoate, generates more efficient compounds than those bearing the electron-rich *p*-cymene ring. Thus, η^6-arene ligands with different donating and/or withdrawing substituents may be used to adjust the biological properties of the corresponding Ru complexes.

(ii) Their $PR^1R^2R^3$ ligand. Many P-substituents can be used; it has been shown that the sole replacement of a phenyl group by a methyl one leads to a drastic modification of the biological behavior of the resulting Ru complexes. Hence, this provides immense opportunities to develop

DOI: 10.1021/acs.inorgchem.8b02541
Inorg. Chem. XXXX, XXX, XXX−XXX

new members of this family of piano-stool compounds with improved properties.

It can also be mentioned that both the η^6-arene and $PR^1R^2R^3$ ligands may be used to introduce functional groups for the targeting or/and delivery of the cytotoxic agent, hence increasing its selectivity and efficiency. Finally, the anionic ligands (viz. the chlorides in the complexes described herein) may also be replaced by other anions, thus providing an additional option/tool for the tuning of the biological properties of the complexes; actually, this is currently being investigated.

EXPERIMENTAL SECTION

General. Ethidium bromide, sodium cacodylate, tris acetate-ethylenediaminetetraacetic acid (TAE), cisplatin, 3-(4,5-dimethylthiazol-2-yl)-2,5-diphenyltetrazolium bromide (MTT), and *calf thymus* DNA (ct-DNA) were obtained from Sigma-Aldrich. Plasmid pBR322 DNA was purchased from Fisher Scientific. All compounds used for the DNA interaction studies (fluorescence and gel electrophoresis) were acquired from Sigma-Aldrich and Invitrogen. All the ligands and ruthenium complexes were prepared under a purified nitrogen atmosphere using standard Schlenk and vacuum-line techniques. The solvents were obtained from a solvent purification system or purified by standard procedures.[49] ^{1}H, ^{13}C{^{1}H}, and ^{31}P{^{1}H} and HSQC ^{1}H–^{13}C NMR spectra were recorded at 298 K on a Varian Mercury 400 MHz spectrometer using $CDCl_3$ as solvent. Chemical shifts (δ) are reported in parts per million (ppm) and are referenced to the nondeuterated solvent peak ($CHCl_3$: 7.26 ppm). The protons of the BH_3 group of phosphine-borane **L1′** (Scheme 2) appeared in the aliphatic region of the spectra as very broad signals and have not been assigned. IR spectra were recorded in KBr using a Nicolet-5700 FT-IR (in the range 4000–400 cm^{-1}), and the main absorption bands are reported (cm^{-1}). High-resolution mass analyses were carried out at the Centres Cientifics i Tecnologics de la Universitat de Barcelona, with a time-of-flight instrument using electrospray ionization. C, H, and N elemental analyses were performed at the Centres Cientifics i Tecnologics de la Universitat de Barcelona, using a Thermo EA 1108 CHNS/O analyzer from Carlo Erba Instruments. Spectroscopic measurements (DNA-binding studies) were performed in cacodylate buffer solution (1 mM sodium cacodylate, 20 mM NaCl, pH 7.2), prepared with ultrapure water and whose pH was adjusted with aqueous HCl. The concentration of ct-DNA/plasmid DNA was determined from its absorption intensity at 260 nm with a molar extinction coefficient of 6600 $M^{-1}cm^{-1}$. The DNA purity was determined through the 260 nm/280 nm ratio (a ratio around 1.8–1.9 indicates that the DNA used is sufficiently protein free). Fluorescence spectra were collected in 1 cm path length quartz cuvettes using a Horiba Jovin Yvon iHR320 spectrofluorometer.

The dimeric ruthenium precursor **DB**[50] (Scheme 2), ligand *S*-**L3**,[30] and complex **5**[30] were prepared following published procedures.

Preparation of Ligands. *Dimethyl(1-pyrenyl)phosphane-borane (**L1′**).* 1-Bromopyrene (1.69 g, 6.0 mmol) was dissolved in 20 mL of THF, and the solution was cooled to −78 °C. To the cold solution, 1.6 M *n*-BuLi in hexane (3.6 mL, 5.7 mmol) was added using a syringe, and the resulting mixture was stirred for 1 h. To the organolithium solution, chlorodimethylphosphane (0.41 mL, 500 mg, 5.2 mmol) was added, and the reaction mixture was allowed to warm up to room temperature for 14 h. 1 M borane-THF (10 mL, 10.0 mmol) was added, and the resulting solution was stirred for 1 h. Water (10 mL) was carefully added, and the THF was removed under reduced pressure. After extraction with dichloromethane (3 × 10 mL), the combined organic phases were washed with 20 mL of water. The final organic phase was dried with anhydrous sodium sulfate and filtered, and the solvent was removed under reduced pressure giving the crude product, which was purified by column chromatography (flash SiO_2, hexane/ethyl acetate 95:5). **L1′** was obtained as a white solid (589 mg, 41%). ^{1}H NMR ($CDCl_3$, 400 MHz): δ = 8.74 (d, J = 9.2, 1H), 8.36 (dd, J = 12.4, 8.0, 1H), 8.30–8.27 (m, 3H), 8.20 (dd, J = 8.0, 1.6, 1H), 8.17 (d, J = 8.8, 1H), 8.08 (d, J = 7.6, 1H), 8.07 (d, J = 8.8, 1H), 1.93 (d, $^2J_{HP}$ = 10.0, 6H). ^{13}C{^{1}H} NMR ($CDCl_3$, 101 MHz): δ = 133.7–123.3 (C, CH, Ar), 13.9 (d, $^1J_{CP}$ = 39.6, $2CH_3$). ^{31}P{^{1}H} NMR ($CDCl_3$, 162 MHz): δ = +1.8 (d, br, $^1J_{BP}$ = 68.7). HRMS: calcd. for $C_{18}H_{22}BNP$ ([M] + NH_4), 294.1577; found, 294.1573.

*Dimethyl(1-pyrenyl)phosphane (**L1**).* **L1′** (250 mg, 0.91 mmol) was dissolved in 20 mL of dichloromethane, and the solution was cooled to 0 °C. Subsequently, $HBF_4{\cdot}Et_2O$ (0.62 mL, 4.5 mmol) was added, and the resulting mixture was stirred for 1 h. Ten milliliters of a thoroughly deoxygenated saturated aqueous solution of $NaHCO_3$ were carefully added to the formed phosphonium salt. The organic layer was transferred to another flask, washed with thoroughly deoxygenated water, dried with sodium sulfate, and filtered, and the solvent was evaporated under reduced pressure. **L1** was obtained as an air-sensitive colorless oil (208 mg, 87%). ^{1}H NMR ($CDCl_3$, 400 MHz): δ = 8.86 (dd, J = 9.2, 5.2, 1H), 8.23–8.00 (m, 8H), 1.55 (d, $^2J_{HP}$ = 2.8, 6H). ^{13}C{^{1}H} NMR (101 MHz): δ = 133.3–124.7 (C, CH, Ar), 14.1 (d, $^1J_{CP}$ = 10.9, $2CH_3$). ^{31}P{^{1}H} NMR (162 MHz): δ = −59.6 (s).

*Diphenyl(1-pyrenyl)phosphane (**L2**).* 1-Bromopyrene (492 mg, 1.75 mmol) was dissolved in 20 mL of THF, and the solution was cooled to −78 °C. 1.6 M *n*-BuLi in hexane (1.0 mL, 1.60 mmol) was then added using a syringe, and the reaction mixture was stirred for 1 h. Next, chlorodiphenylphosphane (0.25 mL, 300 mg, 1.35 mmol) was added to the organolithium solution, and the resulting mixture was allowed to warm up to room temperature. After 14 h, water (10 mL) was carefully added, and THF was removed under reduced pressure. The resulting aqueous phase was extracted with dichloromethane (3 × 10 mL), and the combined organic phase was washed with 20 mL of water. The organic phase was then dried over anhydrous sodium sulfate and filtered, and the solvent was removed under reduced pressure. **L2** was obtained as a white solid (450 mg, 87%). The characterization data match those reported earlier for this compound.[26] 1H NMR ($CDCl_3$, 400 MHz): δ = 8.77 (dd, J = 9.2, 4.8, 1H), 8.21 (dd, J = 4.4, 0.8, 1H), 8.19 (d, J = 3.6, 1H), 8.12–8.00 (m, 5H), 7.55 (dd, J = 8.0, 4.4, 1H), 7.35–7.32 (m, 10H). ^{31}P{^{1}H} NMR (162 MHz): δ = −14.0 (s).

Preparation of Ruthenium Compounds. *[Ru(η^6-*p*-cymene)-Cl_2(**L1**)] (**1**).* Procedure **A** (see Scheme 3): **L1** (200 mg, 0.76 mmol) was dissolved in 10 mL of dichloromethane and [RuCl(μ-Cl)(η^6-*p*-cymene)]$_2$ (**DC**; 195 mg, 0.32 mmol) was subsequently added. The resulting red solution was stirred for 1 h protected from light, and the solvent was removed under reduced pressure. The residue was recrystallized from dichloromethane/hexane, producing pure **1** as a dark-red solid (198 mg, 55%).

Procedure **B** (see Scheme 3): 1-Bromopyrene (1.69 g, 6.0 mmol) was dissolved in 20 mL of THF, and the resulting solution was cooled to −78 °C. Next, 1.6 M *n*-BuLi in hexane (3.6 mL, 5.7 mmol) was added using a syringe, and the reaction mixture was stirred for 1 h. Chlorodimethylphosphane (0.41 mL, 500 mg, 5.2 mmol) was subsequently added to the organolithium solution, and the mixture was allowed to warm up to room temperature. After 16 h, 1 mL of methanol was added, and the solvent was evaporated under reduced pressure. The ensuing crude solid was dissolved in 20 mL of CH_2Cl_2 and **DC** (350 mg, 0.57 mmol) was added. The resulting orange solution was stirred for 1 h protected from light and was rapidly washed with water (2 × 10 mL). The organic phase was dried over anhydrous sodium sulfate and filtered. After evaporation of the solvent under reduced pressure, the solid residue was recrystallized from dichloromethane/hexane, producing **1** as a dark-red compound (590 mg, 90%).

IR (KBr, cm^{-1}): 3040, 2958, 2915, 1593, 1460, 1415, 1381, 1293, 1279, 1213, 1084, 1057, 1031, 949, 916, 845, 718, 701. ^{1}H NMR ($CDCl_3$, 400 MHz): δ = 9.17 (d, J = 9.2, 1H), 8.41 (dd, J = 9.6, 8.0, 1H), 8.32–8.28 (m, 4H), 8.22 (d, J = 8.8, 1H), 8.15 (d, J = 8.9, 1H), 8.10 (d, J = 7.6, 1H), 5.12 (d, J = 5.6, 2H), 4.78 (s, br, 2H), 2.75 (h, $^3J_{HH}$ = 6.8, 1H), 2.06 (s, br, 6H), 1.80 (s, 3H), 1.14 (d, $^3J_{HH}$ = 6.8, 6H). ^{13}C{^{1}H} NMR (101 MHz): δ = 133.2–124.0 (C, CH, Ar), 107.3 (s, 2CH), 96.5 (s, 2CH), 30.5 (s, CH), 22.2 (s, $2CH_3$), 18.1 (s,

DOI: 10.1021/acs.inorgchem.8b02541
Inorg. Chem. XXXX, XXX, XXX–XXX

CH_3), 14.1 (s, br, CH_3). $^{31}P\{^1H\}$ NMR (162 MHz): δ = +7.7 (s). HRMS: calcd. for $C_{34}H_{45}NPCl_2Ru$ ([M] + NEt_3), 670.1704; found, 670.1711. C, H Anal.: cald. for $C_{28}H_{29}Cl_2PRu$, C 59.16%, H 5.14%; found, C 57.89%, H 5.32%.

*[Ru(η^6-methyl benzoate)Cl_2(**L1**)] (**2**).* Procedure **A**: **L1** (200 mg, 0.76 mmol) was dissolved in 10 mL of dichloromethane and $[RuCl(\mu\text{-}Cl)(\eta^6\text{-methyl benzoate})]_2$ (**DB**; 196 mg, 0.32 mmol) was subsequently added. The resulting red solution was stirred for 1 h protected from light and subsequently filtered; the solvent was then removed under reduced pressure. The solid residue was recrystallized from dichloromethane/hexane to give pure **2** as a dark-red solid (280 mg, 77%).

Procedure **B**: the method applied for **1** was followed (see above) using 1.69 g (6.00 mmol) of 1-bromopyrene, 3.6 mL (5.7 mmol) of 1.6 M *n*-BuLi in hexane, 0.4 mL (500 mg, 5.20 mmol) of chlorodimethylphosphane and 388 mg (0.63 mmol) of **DB**. After workup and recrystallization, pure **2** was obtained a dark-red solid (680 mg, 94%).

IR (KBr, cm^{-1}): 3081, 2953, 1701 ν(C = O), 1592, 1518, 1422, 1292, 1272, 1110, 949, 917, 850, 773, 720. ^1H NMR ($CDCl_3$, 400 MHz): δ = 9.11 (d, J = 9.2, 1H), 8.49 (dd, J = 10.0, 8.0, 1H), 8.35−8.30 (m, 4H), 8.24 (d, J = 8.8, 1H), 8.17 (d, J = 8.8, 1H), 8.12 (d, J = 8.1, 1H), 6.25 (s, br, 2H), 5.47 (t, J = 5.2, 1H), 3.88 (s, 3H), 2.06 (s, br, 6H). $^{13}C\{^1H\}$ NMR (101 MHz): δ = 165.5 (s, C = O), 133.5−124.1 (C, CH, Ar), 92.4 (s, 2CH), 79.8 (s, CH), 53.2 (s, CH_3), 13.5 (m, br, $2CH_3$). $^{31}P\{^1H\}$ NMR (162 MHz): δ = +9.6 (s). HRMS: calcd. for $C_{32}H_{39}NO_2PCl_2Ru$ ([M] + NEt_3), 672.1133; found, 672.1143. Anal.: cald. for $C_{26}H_{23}Cl_2O_2PRu$, C 54.75%, H 4.06%; found, C 52.99%, H 4.35%.

*[Ru(η^6-*p*-cymene)Cl_2(**L2**)] (**3**).* Procedure **A**: the synthetic procedure used to prepare **1** was followed with 173 mg (0.45 mmol) of **L2** and 114 mg (0.19 mmol) of **DC**. Pure **3** was obtained as a dark-red solid (237 mg, 90%).

Procedure **B**: the synthetic procedure applied for **1** was used with 500 mg (1.79 mmol) of 1-bromopyrene, 1.0 mL (1.6 mmol) of 1.6 M *n*-BuLi in hexane, 0.2 mL (290 mg, 1.36 mmol) of chlorodimethylphosphane and 420 mg (0.69 mmol) of **DC**. Pure **3** was obtained as a dark-red solid (890 mg, 94%).

IR (KBr, cm^{-1}): 3041, 2958, 2923, 2869, 1581, 1481, 1468, 1434, 1374, 1207, 1189, 1159, 1091, 1028, 857, 751, 741, 720, 692, 634, 606, 582, 540, 516, 465, 425. ^1H NMR ($CDCl_3$, 400 MHz): δ = 8.90 (d, J = 9.6, 1H), 8.29 (t, J = 8.0, 2H), 8.23 (d, J = 9.2, 1H), 8.14−8.08 (m, 4H), 7.74 (t, J = 10.4, 1H), 7.66 (t, J = 8.8, 4H), 7.37−7.26 (m, 6H), 5.29 (s, 2H), 4.47 (s, br, 2H), 3.12 (h, $^3J_{HH}$ = 6.8, 1H), 1.62 (s, 3H), 1.26 (d, $^3J_{HH}$ = 6.8, 6H). $^{13}C\{^1H\}$ NMR (101 MHz): δ = 135.7−123.7 (C, CH, Ar), 113.6 (d, $^2J_{CP}$ = 6.5, C), 98.3 (s, C), 88.6 (s, 2CH), 86.3 (s, 2CH), 30.5 (s, CH), 22.1 (s, $2CH_3$), 18.2 (s, CH_3). $^{31}P\{^1H\}$ NMR (162 MHz): δ = +32.1 (s). HRMS: calcd. for calcd. for $C_{38}H_{37}NPCl_2Ru$ ([M] + NH_4), 710.1078; found, 710.1073. Anal.: cald. for $C_{38}H_{33}Cl_2PRu$, C 65.90%, H 4.80%; found, C 65.00%, H 5.11%.

*[Ru(η^6-methyl benzoate)Cl_2(**L2**)] (**4**).* Procedure **A**: 200 mg (0.52 mmol) of ligand **L2** was dissolved in 10 mL of dichloromethane, and 185 mg (0.30 mmol) of **DB** was added. The resulting red solution was stirred for 1 h protected from light and subsequently filtered, and the solvent was removed under reduced pressure. The solid residue was recrystallized from dichloromethane/hexane, giving pure **4** as a dark-red solid (300 mg, 83%).

Procedure **B**: the method applied for **1** was followed (see above) using 500 mg (1.79 mmol) of 1-bromopyrene, 1.0 mL (1.60 mmol) of 1.6 M *n*-BuLi in hexane, 0.2 mL (290 mg, 1.36 mmol) of chlorodimethylphosphane and 420 mg (0.68 mmol) of **DB**. Pure **4** was obtained as a dark-red solid (900 mg, 95%).

IR (KBr, cm^{-1}): 3059, 2949, 1717 ν(C = O), 1657, 1556, 1451, 1271, 1106, 843, 856, 704. ^1H NMR ($CDCl_3$, 400 MHz): δ = 8.81 (d, J = 9.2, 1H), 8.31 (d, J = 8.0, 1H), 8.29 (d, J = 8.0, 1H), 8.24 (d, J = 8.8, 1H), 8.14 (d, J = 2.8, 2H), 8.12 (d, J = 2.8, 2H), 7.61−7.56 (m, 5H), 7.41 (s, br, 3H), 7.31 (s, br, 3H), 6.44 (d, J = 6.0, 2H), 4.89 (s, br, 3H), 4.75−4.71 (m, 2H), 3.91 (s, 3H). $^{13}C\{^1H\}$ NMR (101 MHz): δ = 164.2 (s, C = O), 135.6−124.0 (C, CH, Ar), 89.6 (s, CH), 53.5 (s, CH_3). $^{31}P\{^1H\}$ NMR (162 MHz): δ = +32.1 (s). HRMS: calcd. for calcd. for $C_{36}H_{31}Cl_2NO_2PRu$ ([M] + NH_4), 712.0507; found, 712.0499. Anal.: cald. for $C_{36}H_{27}Cl_2O_2PRu$, C 62.25%, H 3.92%; found, C 59.25%, H 3.95%.

*[Ru(η^6-methyl benzoate)Cl_2(*S*-**L3**)] (**6**).* The procedure **A** applied to prepare **2** was followed (see above) using 388 mg (1.20 mmol) of *S*-**L3** and 308 mg (0.50 mmol) of **DB**. Pure **6** was obtained as a dark-red solid (571 mg, 90%).

IR (KBr, cm^{-1}): 3052, 2949, 1727 ν(C = O), 1581, 1520, 1486, 1434, 1293, 1275, 1109, 895, 851, 768, 749, 720, 691, 629, 602, 499. ^1H NMR ($CDCl_3$, 400 MHz): δ = 8.59 (t, J = 7.6, 1H), 8.43 (d, J = 9.2, 1H), 8.37 (d, J = 7.2, 1H), 8.30−8.17 (m, 4H), 8.09 (d, J = 7.6, 1H), 8.04 (d, J = 9.6, 1H), 7.66 (t, J = 8.4, 1H), 7.35 (t, J = 6.4, 1H), 7.26 (m, 2H), 6.47 (s, br, 1H), 6.09 (s, br, 1H), 5.43 (s, br, 1H), 5.36 (s, br, 1H), 4.55 (s, br, 1H), 3.86 (s, 3H), 2.36 (d, $^2J_{HP}$ = 10.8, 3H). $^{13}C\{^1H\}$ NMR (101 MHz): δ = 164.8 (s, C = O), 133.6−124.2 (C, CH, Ar), 97.2 (s, CH), 91.5 (s, CH), 90.7 (s, CH), 87.7 (s, CH), 84.0 (s, CH), 53.2 (s, CH_3), 16.0 (d, $^1J_{CP}$ = 36.1, CH_3). $^{31}P\{^1H\}$ NMR (162 MHz): δ = +16.6 (s). HRMS: calcd. for calcd. for $C_{31}H_{29}NO_2PCl_2Ru$ ([M] + NH_4), 650.0349; found, 650.0354. Anal.: cald. for $C_{31}H_{25}Cl_2O_2PRu$, C 58.87%, H 3.98%; found, C 57.86%, H 4.12%.

X-ray Structure Determination. Single crystals, suitable for X-ray diffraction studies, of **1**, **2**, and **4** were obtained by slow diffusion of hexane into a dichloromethane solution of each complex, at 4 °C. Crystallographic data for **1**, **2**, and **4** were collected on a Bruker APEX II QUAZAR diffractometer equipped with a microfocus multilayer monochromator with Mo Kα radiation (λ = 0.71073 Å), at the Group of Magnetism and Functional Molecules (GMMF) of the Universitat de Barcelona. Data reduction and absorption corrections were performed by using SAINT and SADABS (Bruker AXS Inc., Madisson, Wisconsin, USA), respectively. The structures were solved using SHELXT[51,52] and refined with OLEX2[53] suite. Crystallographic and refinement parameters for the three compounds are summarized in Table S1. All details can be found in CCDC 1863809 (**1**), 1863807 (**2**), and 1863808 (**4**) that contain the supplementary crystallographic data for this paper. These data can be obtained free of charge from the Cambridge Crystallographic Data Center via https://summary.ccdc.cam.ac.uk/structure-summary-form.

Agarose Gel Electrophoresis. Twenty microliters of cacodylate-buffered solutions of pBR322 plasmid DNA (15 μM, in base pair) containing 0.42, 0.83, 1.67, and 3.33 equiv of the complexes (6.25−50 μM, obtained from DMSO stock solutions) were incubated for 24 h at 37 °C. Control samples of free DNA and DNA bound to cisplatin (0.5 and 1 equiv) were also prepared. Following the incubation, 4 μL of a xylene cyanol 0.25% aqueous solution (containing 30% glycerol) was added to all samples, which were subsequently electrophoretized in agarose gel (1% in TBE buffer) for 1 h at 6.25 V cm^{-1}, using a Bio-Rad horizontal tank connected to a Consort EV231 variable potential power supply. The gel was then treated with SYBR Safe DNA gel stain and consequently photographed with a Bio-Rad Gel Doc EZ imager.

Ethidium Bromide Displacement Assays. Samples containing ct-DNA (15 μM, in base pair) and ethidium bromide (ethidium bromide, EB; 75 μM) in cacodylate buffer (1 mM sodium cacodylate, 20 mM NaCl, pH = 7.2) were incubated at 37 °C for 1 h. Then, the samples were treated with increasing amounts of 250 μM stock solutions of the complexes freshly prepared in DMSO (final complex concentrations of 1, 2, 3, 6, 9, 12, 15, 20, and 25 μM were used for the experiments). The optimum DNA/EB ratio of 1:5 was determined experimentally, by fluorescence spectroscopy. This ratio corresponds to the saturation of the emission signal, illustrated by a plateau and is indicative of the occupation of all possible intercalation sites by EB. The samples, containing 1−25 μM of the complexes investigated and up to a maximum of 5% DMSO in a final volume of 3 mL, were subsequently incubated at 37 °C for 24 h. The fluorescence emission spectra of all samples were then recorded at room temperature in the range 520−700 nm, applying an excitation wavelength λ_{exc} = 514 nm. Blank experiments were also carried out with cacodylate-buffered solutions of ct-DNA/EB (namely, without complex).

DOI: 10.1021/acs.inorgchem.8b02541
Inorg. Chem. XXXX, XXX, XXX−XXX

Cell Lines and Culture. The A549 (lung adenocarcinoma), A375 (melanoma), SW620 (colorectal adenocarcinoma), MCF7 (breast carcinoma), MCF10A (nontumorigenic mammary epithelial), SK-N-BE(2) (neuroblastoma), and CHLA-90 (neuroblastoma) human cell lines were purchased from the American Type Culture Collection (ATCC, Manassas, VA, USA). All cell lines were tested and verified by ATCC using short tandem repeat analysis and were cultured (passage number 10−25) using ATCC recommended media. Hence, A549, A375, and SW620 cells were cultured in Dulbecco's Modified Eagle's Medium (DMEM) medium supplemented with 10% (v/v) heat-inactivated fetal bovine serum (FBS; Life Technologies, Carlsbad, CA, USA), 100 unit/mL penicillin, 100 μg/mL streptomycin, and 2 mM L-glutamine. MCF7 and MCF10A cells were cultured in DMEM-F12 (DMEM/nutrient mixture F-12 Ham) medium (1:1) supplemented with 10% FBS or 5% horse serum (v/v), respectively, 100 μM sodium pyruvate, 10 μg/mL insulin, 100 unit/mL penicillin, 100 μg/mL streptomycin, and 2 mM L-glutamine. Moreover, MCF10A cells were supplemented with 20 ng/mL epidermal growth factor (EGF, Sigma-Aldrich), 0.5 μg/mL hydrocortisone, and 100 ng/mL cholera toxin. SK-N-BE(2) and CHLA-90 cells were cultured in Iscove's modified Dulbecco's media (IMDM), supplemented with 20% FBS, 1% insulin-transferrin-selenium (ITS, Life Technologies), 100 unit/mL penicillin, and 100 μg/mL streptomycin.

All cell lines were grown at 37 °C under an atmosphere containing 5% CO_2. The cell lines were routinely tested using a specific standard PCR to control mycoplasma contamination.

Cell Viability Assays. Cell proliferation was evaluated by the MTT assay. The cells (1×10^5 cells per mL) were plated in 96-well sterile plates and allowed to grow for 24 h. After attachment to the surface, the cells were subsequently incubated for 24 h at 37 °C, with various concentrations of the ruthenium(II) compounds (0.4−50 μM for compound **1**, 0.2−20 μM for compound **2**, 0.8−100 μM for compounds **3** and **4**, and 0.5−5 μM for compounds **5** and **6**), freshly prepared from stock solutions in DMSO and diluted in the corresponding culture medium (the final concentration of DMSO was of 1%). Control cells (namely, without added compound) were cultured in the corresponding culture medium plus the carrier, viz. 1% DMSO. Following the incubation, 10 μM MTT were added to each well, and the cells were further incubated for 2 h. Next, the medium was aspirated, and the blue formazan precipitate was dissolved in 100 μL of DMSO. The absorbance at 570 nm was registered using a multiwell plate reader (Multiskan FC, Thermo Scientific). The cell viability was expressed as percentage values with respect to control cells, and the data are given as the mean value ± SD (standard deviation) of three independent experiments. Dose−response curves and the corresponding IC_{25}, IC_{50}, and IC_{75} values were obtained through nonlinear regression (curve fit), calculated with the GraphPad Prism 5.0 software.

Flow Cytometry − Cell Cycle and Apoptosis. A375 cells (2×10^5 cells) were seeded in six-well plates and, after 24 h, they were treated with IC_{50} values of compounds **1**−**6** for 24 h. Similarly, control cells were treated with 1% DMSO, and positive controls were also treated with cisplatin (5 μM for 48 h) or staurosporine (200 nM for 24 h). Afterward, the cells were detached, centrifuged at 300 g for 5 min, and resuspended in 1 mL of 1× PBS-1% FBS. Then, for the assessment of apoptosis, 100 μL of cell suspension were mixed with Annexin-V kit buffer (1:1; Muse Annexin V & Dead Cell Assay, Merck Millipore, Merck KGaA, Darmstadt, Germany). After 20 min of incubation at room temperature, the cells were examined on the Muse Cell analyzer (Merck Millipore). During the incubation time, the cells for the cell cycle analysis were prepared. The rest of the cell suspension (900 μL) was centrifuged at 300*g* for 5 min and resuspended in 50 μL of PBS. The cells were slowly added, drop by drop, to 1 mL of ice cold 70% ethanol and were incubated overnight at −20 °C. The next day, 500 μL of cell suspension were centrifuged at 300*g* for 5 min, washed once with 1× PBS, and resuspended in a final volume of 200 μL. Finally, 200 μL of Muse Cell Cycle reagent was added and incubated for 30 min in the dark. Afterward, the cells were examined on the Muse Cell analyzer. All the conditions were assessed in three independent experiments. The results are shown as the mean value ± SD.

Wound-Healing Assay. 1×10^5 cells per mL were seeded in a 12-well plate and allowed to grow for 24 h (during this time, the cells reached a density of ca. 80%). Cell division (proliferation) was inhibited by adding 10 μg/mL mitomycin C. Following the incubation, an incision/scratch was established in the central area by using a sterile pipet tip. The cells were then treated with each compound, and images were regularly taken using a phase-contrast light microscope (Axio Observer Z1, Göttingen, Germany). The migration of cells in the wound space, i.e., the wound closure, was quantified using the MRI Wound Healing Tool macro for ImageJ (see http://dev.mri.cnrs.fr/projects/imagej-macros/wiki/Wound_Healing_Tool). The results are expressed as the mean ± SEM (standard error of mean) of three independent experiments. One-way ANOVAs were carried out with the Statgraphics Centurion statistical package (StatPoint, Inc., Herndon, VA, USA), and the posthoc Tukey test was applied.

■ ASSOCIATED CONTENT

Supporting Information

The Supporting Information is available free of charge on the ACS Publications website at DOI: 10.1021/acs.inorgchem.8b02541.

Representation of the structures of **1**−**6** (Scheme S1); crystal data and structure refinement for compounds **1**, **2**, and **4** (Table S1); specific angles for the phosphane ligand in **1**, **2**, and **4** (Table S2); crystal packings for **2** and **4** (Figures S1 and S2, respectively); agarose gel electrophoresis images for **2**−**6** (Figure S3); ethidium-bromide displacement data for **1**−**6** (Figure S4); stability studies of **2** and **1** in DMSO using ^{1}H NMR (Figures S5 and S6, respectively); representation of the chemical structure of irinotecan and its metabolite **SN-38** (Figure S7); wound-healing images for **1** and **2** (Figures S8 and S9, respectively); IC_{25}, IC_{50}, and IC_{75} data for **1**−**6** against five cell lines, namely, A549 (lung adenocarcinoma), A375 (melanoma), SW620 (colorectal adenocarcinoma), MCF7 (breast carcinoma), and MCF10A (nontumorigenic mammary epithelial) (Tables S3−S7, respectively) (PDF)

Accession Codes

CCDC 1863807−1863809 contain the supplementary crystallographic data for this paper. These data can be obtained free of charge via www.ccdc.cam.ac.uk/data_request/cif, or by emailing data_request@ccdc.cam.ac.uk, or by contacting The Cambridge Crystallographic Data Centre, 12 Union Road, Cambridge CB2 1EZ, UK; fax: +44 1223 336033.

■ AUTHOR INFORMATION

Corresponding Authors

*(A.G.) E-mail: arnald.grabulosa@qi.ub.es.
*(P.G.) E-mail: patrick.gamez@qi.ub.es.

ORCID

Arnald Grabulosa: 0000-0003-0198-4139
Patrick Gamez: 0000-0003-2602-9525

Notes

The authors declare no competing financial interest.

■ ACKNOWLEDGMENTS

Financial support from the Spanish Ministerio de Ciencia Innovación, y Universidades (Project Nos. CTQ2015-70371 and CTQ2017-88446-R AEI/FEDER, UE) is acknowledged.

DOI: 10.1021/acs.inorgchem.8b02541
Inorg. Chem. XXXX, XXX, XXX−XXX

P.G. acknowledges the Institució Catalana de Recerca i Estudis Avançats (ICREA). Also, an individual contract to L.K.G. supported by a program from the Barcelona University in collaboration with Obra Social de la Fundació Bancaria "La Caixa" is acknowledged. The authors thank Jorge Salinas-Uber, George Manganas, Nora O'Gorman, and Susan Humphreys for the analytical data obtained for some of the compounds described in the present manuscript.

REFERENCES

(1) Siegel, R. L.; Miller, K. D.; Jemal, A. Cancer Statistics, 2017. *Ca-Cancer J. Clin.* **2017**, *67*, 7−30.
(2) Rosenberg, B.; Vancamp, L.; Trosko, J. E.; Mansour, V. H. Platinum Compounds - A New Class of Potent Antitumour Agents. *Nature* **1969**, *222*, 385−386.
(3) Dasari, S.; Tchounwou, P. B. Cisplatin in cancer therapy: Molecular mechanisms of action. *Eur. J. Pharmacol.* **2014**, *740*, 364−378.
(4) Kelland, L. The resurgence of platinum-based cancer chemotherapy. *Nat. Rev. Cancer* **2007**, *7*, 573−584.
(5) Housman, G.; Byler, S.; Heerboth, S.; Lapinska, K.; Longacre, M.; Snyder, N.; Sarkar, S. Drug Resistance in Cancer: An Overview. *Cancers* **2014**, *6*, 1769−1792.
(6) Rothenberg, M. L.; Carbone, D. R.; Johnson, D. H. Improving the evaluation of new cancer treatments: challenges and opportunities. *Nat. Rev. Cancer* **2003**, *3*, 303−309.
(7) Saborit, J. M.; Caubet, A.; Brissos, R. F.; Korrodi-Gregorio, L.; Perez-Tomas, R.; Martinez, M.; Gamez, P. pH-Driven preparation of two related platinum(II) complexes exhibiting distinct cytotoxic properties. *Dalton Trans.* **2017**, *46*, 11214−11222.
(8) Medici, S.; Peana, M.; Nurchi, V. M.; Lachowicz, J. I.; Crisponi, G.; Zoroddu, M. A. Noble metals in medicine: Latest advances. *Coord. Chem. Rev.* **2015**, *284*, 329−350.
(9) Grau, J.; Renau, C.; Caballero, A. B.; Caubet, A.; Pockaj, M.; Lorenzo, J.; Gamez, P. Evaluation of the metal-dependent cytotoxic behaviour of coordination compounds. *Dalton Trans* **2018**, *47*, 4902−4908.
(10) Fricker, S. P. Metal based drugs: from serendipity to design. *Dalton Trans* **2007**, 4903−4917.
(11) Cuello-Garibo, J.-A.; James, C. C.; Siegler, M. A.; Bonnet, S. Ruthenium-based PACT compounds based on an N,S non-toxic ligand: a delicate balance between photoactivation and thermal stability. *Chem. Sq.* **2017**, *1*, 2.
(12) Chow, M. J.; Alfiean, M.; Pastorin, G.; Gaiddon, C.; Ang, W. H. Apoptosis-independent organoruthenium anticancer complexes that overcome multidrug resistance: self-assembly and phenotypic screening strategies. *Chem. Sci.* **2017**, *8*, 3641−3649.
(13) Gasser, G.; Ott, I.; Metzler-Nolte, N. Organometallic Anticancer Compounds. *J. Med. Chem.* **2011**, *54*, 3−25.
(14) Süss-Fink, G. Arene ruthenium complexes as anticancer agents. *Dalton Trans* **2010**, *39*, 1673−1688.
(15) Murray, B. S.; Babak, M. V.; Hartinger, C. G.; Dyson, P. J. The development of RAPTA compounds for the treatment of tumors. *Coord. Chem. Rev.* **2016**, *306*, 86−114.
(16) Hartinger, C. G.; Metzler-Nolte, N.; Dyson, P. J. Challenges and Opportunities in the Development of Organometallic Anticancer Drugs. *Organometallics* **2012**, *31*, 5677−5685.
(17) Scolaro, C.; Bergamo, A.; Brescacin, L.; Delfino, R.; Cocchietto, M.; Laurenczy, G.; Geldbach, T. J.; Sava, G.; Dyson, P. J. In vitro and in vivo evaluation of ruthenium(II)-arene PTA complexes. *J. Med. Chem.* **2005**, *48*, 4161−4171.
(18) Allardyce, C. S.; Dyson, P. J.; Ellis, D. J.; Heath, S. L. [Ru(eta(6)-p-cymene)Cl-2(pta)] (pta = 1,3,5-triaza-7-phosphatricyclo[3.3.1.1]decane): a water soluble compound that exhibits pH dependent DNA binding providing selectivity for diseased cells. *Chem. Commun.* **2001**, 1396−1397.
(19) Biancalana, L.; Pampaloni, G.; Marchetti, F. Arene Ruthenium-(II) Complexes with Phosphorous Ligands as Possible Anticancer Agents. *Chimia* **2017**, *71*, 573−579.
(20) Chaplin, A. B.; Dyson, P. J. Influence of arene dissociation and phosphine coordination on the catalytic activity of [RuCl(kappa(2)-triphos)(p-cymene)]PF6. *J. Organomet. Chem.* **2011**, *696*, 2485−2490.
(21) Betanzos-Lara, S.; Novakova, O.; Deeth, R. J.; Pizarro, A. M.; Clarkson, G. J.; Liskova, B.; Brabec, V.; Sadler, P. J.; Habtemariam, A. Bipyrimidine ruthenium(II) arene complexes: structure, reactivity and cytotoxicity. *JBIC, J. Biol. Inorg. Chem.* **2012**, *17*, 1033−1051.
(22) Harvey, R. G. Polycyclic Aromatic Hydrocarbons. In *Cambridge Monographs on Cancer Research*; Cambridge University Press: Cambridge, 1991.
(23) Sola, M. Forty years of Clar's aromatic pi-sextet rule. *Front. Chem.* **2013**, *1*, 8.
(24) Lou, C.; Dallmann, A.; Marafini, P.; Gao, R.; Brown, T. Enhanced H-bonding and pi-stacking in DNA: a potent duplex-stabilizing and mismatch sensing nucleobase analogue. *Chem. Sci.* **2014**, *5*, 3836−3844.
(25) Willis, B.; Arya, D. P. Triple Recognition of B-DNA by a Neomycin-Hoechst 33258-Pyrene Conjugate. *Biochemistry* **2010**, *49*, 452−469.
(26) Hu, J.; Yip, J. H. K.; Ma, D. L.; Wong, K. Y.; Chung, W. H. Switching on the Phosphorescence of Pyrene by Cycloplatination. *Organometallics* **2009**, *28*, 51−59.
(27) McKinstry, L.; Livinghouse, T. An Efficient Procedure for the Synthesis of Electron-Rich Bisphosphines Containing Homochiral Backbones. *Tetrahedron Lett.* **1994**, *35*, 9319−9322.
(28) Kendall, A. J.; Zakharov, L. N.; Tyler, D. R. Steric and Electronic Influences of Buchwald-Type Alkyl-JohnPhos Ligands. *Inorg. Chem.* **2016**, *55*, 3079−3090.
(29) Ficks, A.; Clegg, W.; Harrington, R. W.; Higham, L. J. Air-Stable Chiral Primary Phosphines: A,Gateway to MOP Ligands with Previously Inaccessible Stereoelectronic Profiles. *Organometallics* **2014**, *33*, 6319−6329.
(30) Clavero, P.; Grabulosa, A.; Font-Bardia, M.; Muller, G. P-Stereogenic monophosphines with the 2-p-terphenylyl and 1-pyrenyl substituents. Application to Pd and Ru asymmetric catalysis. *J. Mol. Catal. A: Chem.* **2014**, *391*, 183−190.
(31) Grabulosa, A.; Mannu, A.; Mezzetti, A.; Muller, G. Neutral p-cymene ruthenium complexes with P-stereogenic monophosphines. New catalytic precursors in enantioselective transfer hydrogenation and cyclopropanation. *J. Organomet. Chem.* **2012**, *696*, 4221−4228.
(32) Navarro, M.; Vidal, D.; Clavero, P.; Grabulosa, A.; Muller, G. Mild Photochemical Tethering of [RuCl2(eta(6)-arene)P*] Complexes with P-Stereogenic 2-Biphenylylphosphines. *Organometallics* **2015**, *34*, 973−994.
(33) Clavero, P.; Grabulosa, A.; Rocamora, M.; Muller, G.; Font-Bardia, M. Ruthenium complexes of P-stereogenic phosphines with a heterocyclic substituent. *Dalton Trans* **2016**, *45*, 8513−8531.
(34) Pettinari, R.; Marchetti, F.; Condello, F.; Pettinari, C.; Lupidi, G.; Scopelliti, R.; Mukhopadhyay, S.; Riedel, T.; Dyson, P. J. Ruthenium(II)-Arene RAPTA Type Complexes Containing Curcumin and Bisdemethoxycurcumin Display Potent and Selective Anticancer Activity. *Organometallics* **2014**, *33*, 3709−3715.
(35) Babak, M. V.; Meier, S. M.; Huber, K. V. M.; Reynisson, J.; Legin, A. A.; Jakupec, M. A.; Roller, A.; Stukalov, A.; Gridling, M.; Bennett, K. L.; Colinge, J.; Berger, W.; Dyson, P. J.; Superti-Furga, G.; Keppler, B. K.; Hartinger, C. G. Target profiling of an antimetastatic RAPTA agent by chemical proteomics: relevance to the mode of action. *Chem. Sci.* **2015**, *6*, 2449−2456.
(36) Cohen, G. L.; Bauer, W. R.; Barton, J. K.; Lippard, S. J. Binding of Cis-Dichlorodiammineplatinum(II) And Trans-Dichlorodiammineplatinum(II) To DNA - Evidence for Unwinding and Shortening of The Double Helix. *Science* **1979**, *203*, 1014−1016.
(37) Sherman, S. E.; Lippard, S. J. Structural Aspects of Platinum Anticancer Drug-Interactions With DNA. *Chem. Rev.* **1987**, *87*, 1153−1181.

DOI: 10.1021/acs.inorgchem.8b02541
Inorg. Chem. XXXX, XXX, XXX−XXX

(38) Meyer-Almes, F. J.; Porschke, D. Mechanism of Intercalation into The DNA Double Helix by Ethidium Bromide. *Biochemistry* **1993**, *32*, 4246−4253.
(39) Cuniberti, C.; Guenza, M. Environment-Induced Changes in DNA Conformation as Probed by Ethidium-bromide Fluorescence. *Biophys. Chem.* **1990**, *38*, 11−22.
(40) Kubbies, M.; Goller, B.; Schetters, B.; Bartosek, I.; Albert, W. Glutathione Restores Normal-Cell Activation and Cell-Cycle Progression in Cisplatinum Treated Human-Lymphocytes. *Br. J. Cancer* **1991**, *64*, 843−849.
(41) Lee, S. I.; Brown, M. K.; Eastman, A. Comparison of the efficacy of 7-hydroxystaurosporine (UCN-01) and other staurosporine analogs to abrogate cisplatin-induced cell cycle arrest in human breast cancer cell lines. *Biochem. Pharmacol.* **1999**, *58*, 1713−1721.
(42) Rojas, A.; Figueroa, H.; Morales, E. Fueling inflammation at tumor microenvironment: the role of multiligand/rage axis. *Carcinogenesis* **2010**, *31*, 334−341.
(43) Antonsson, A.; Persson, J. L. Induction of Apoptosis by Staurosporine Involves the Inhibition of Expression of the Major Cell Cycle Proteins at the G(2)/M Checkpoint Accompanied by Alterations in Erk and Akt Kinase Activities. *Anticancer Res.* **2009**, *29*, 2893−2898.
(44) Lanzkowsky, P. *Manual of Pediatric Hematology and Oncology*, 5th ed.; Elsevier, 2011.
(45) Wagner, L. *Neuroblastoma: Diagnosis, Therapy and Prognosis*; Springer Netherlands: Dordrecht, 2012.
(46) Mody, R.; Naranjo, A.; Van Ryn, C.; Yu, A. L.; London, W. B.; Shulkin, B. L.; Parisi, M. T.; Servaes, S. E. N.; Diccianni, M. B.; Sondel, P. M.; Bender, J. G.; Maris, J. M.; Park, J. R.; Bagatell, R. Irinotecan-Temozolomide with temsirolimus or dinutuximab Cross-tafark in children with refractory or relapsed neuroblastoma (COG ANBL1221): an open-label, randomised, phase 2 trial. *Lancet Oncol.* **2017**, *18*, 946−957.
(47) Rothenberg, M. L. Irinotecan (CPT-11): Recent developments and future directions-colorectal cancer and beyond. *Oncologist* **2001**, *6*, 66−80.
(48) Xie, R.; Mathijssen, R. H. J.; Sparreboom, A.; Verweij, J.; Karlsson, M. O. Clinical pharmacokinetics of irinotecan and its metabolites: A population analysis. *J. Clin. Oncol.* **2002**, *20*, 3293−3301.
(49) Armarego, W. L. F.; Chai, C. L. L. *Purification of Laboratory Chemicals*, 7th ed.; Butterworth Heinemann: Oxford, 2013.
(50) Pinto, P.; Marconi, G.; Heinemann, F. W.; Zenneck, U. Chiral arene ruthenium complexes. 6. Diastereoselective formation of chiral-at-metal p-tethered arene ruthenium(II) complexes. *Organometallics* **2004**, *23*, 374−380.
(51) Sheldrick, G. M. A short history of SHELX. *Acta Crystallogr., Sect. A: Found. Crystallogr.* **2008**, *64*, 112−122.
(52) Sheldrick, G. M. *SHELXTL Programs*, http://shelx.uni-goettingen.de/.
(53) Dolomanov, O. V.; Bourhis, L. J.; Gildea, R. J.; Howard, J. A. K.; Puschmann, H. OLEX2: a complete structure solution, refinement and analysis program. *J. Appl. Crystallogr.* **2009**, *42*, 339−341.

DOI: 10.1021/acs.inorgchem.8b02541
Inorg. Chem. XXXX, XXX, XXX−XXX